Ganpat University
॥ विद्यया समाप्नोत्यमृतम् ॥

University Journal of Research
ISSN (Online) 2455-1724

Effects of non-linear radiation and reaction on stagnation point flow of carreau fluid in the presence of magnetic field

Harshad R Patel[a], Rakesh R. Darji[a*]

[a]U. V. P. C. E., Ganpat University, Mehsana, India

Abstract

In this study, mixed convection Magnetohydrodynamics stagnation point flow of Carreau fluid is considered. Flow is two-dimensional and passes through in porous medium. The effects of different physical parameter like, non-linear radiation, chemical reaction and heat generations is studied. The governing equations are transfer in to a system of ODE's using the similarity transformation. The suitable HAM is applied for solution of dimensionless momentum, energy and concentration equations. For better understanding of the problems, the numerical values of skin friction, Nusselt number and Sherwood number is obtained and presented in table. From the graphical results, it is concluded that the motion of fluid improves with increasing the values of magnetic fields, mixed convection parameter and permeability of porous medium parameter. Motion of fluid reduces with rising value of local Weissenberg number. Mass transfer process tends to slow with increasing values of chemical reaction. It is also concluded that the heat transfer process increases with increasing the values of thermal ratio parameter, thermal radiation and heat generation parameter.

Keywords:- MHD; HAM; Mixed Convection; Carreau fluid; Stagnation point flow

1. Introduction

Recently flows of non-Newtonian fluid flow problems with magnetic fields have important role in a various industrial and engineering practices. Carreau fluid one of the generalized Newtonian fluids where viscosity is depended on shear rate. Effect of Carreau fluid flow around around a stretchable cylinder was studied by Jiann et. al. (2024). Vaidya et. al. (2024) discussed the Carreau Yasuda (CY) fluid model. Rehman et. al. (2024) provide analysis based on neural network of heat transfer in MHD thermally slip. Numerical solution of characteristics of Carreau fluid with cross-diffusion effects was discuss by Salahuddin (2024). Ming et. al. (2023) analyses heat transfer effects on Carreau fluid. Many researchers are discussed the effects of different physical parameter on Carreau fluid flow problems (Kudenatti et al., 2023; Almaneera, 2024; Salahuddin et al., 2022a; Khan et al., 2021; Salahuddin et al., 2022b).

Stagnation point flow means the NBHD of stagnation line where stagnation line means the velocity is vanishes in the inviscid approximation. This type of effects is importance in many situations of engineering problems. Li et al. (2024) develop the model of transfer of heat over rotating disk in MHD stagnation point flow. Alqahtani et. al. (2023) compute heat transfer near with non-linear thermal radiation over non-aligned stagnation point. Mittal et al. (2024) identifies chemical reaction on Casson fluid flow. Mittal and Kori (2024) evaluate impact of Dufour-Soret diffusion over viscous sheet. Patel et al. (2024a; 2024b; 2022) studied different physical conditions on nano fluids. Alrehili (2024) discuss dissipative stagnation point flow. Swain et. al. (2024) analyses the effects of heat sink in stagnation point flow which is passes through porous medium whereas, Rafique et. al. (2023) studied radiation effects in fluid flow problems. Analysis of Buoyancy features analysis on MHD stagnation point flow was discuss by Zaheer et. al. (2024) and Baig et. al. (2023). Comparison of analytic and numerical solution for mixed convection stagnation point flow done by Siddiqi et. al. (2023). Waqas et. al. (2021) identifies the numerical solution of bioconvection transport of micropolar nanofluid with thermal radiation. Mittal et al. (2019) studied mixed convection ferrofluid flow with heating. Jalili et. al. (2021) analyses effect of magnetic and boundary parameter of micropolar fluid with thermal radiation. Patel et. al. (2019) discuss MHD over a stretching/shrinking sheet considering radiation. The impact of different physical parameter as well as different physical conditions effects on Carreau fluid of MHD flow

*Corresponding Author
E-mail address: rrd01@ganpatuniversity.ac.in

are discussed many researchers in your works (Kausar, 2022; Khader, 2019; Patel & Singh, 2019; Patel et al., 2022; Simon & Notsu, 2022; Wahid, 2022; Han, 2019).

The aim of the present study is to address the effects of non-linear thermal radiation on stagnation point MHD Carreau fluid flow in porous medium. Additionally, the flow is confined with porous medium and heat generation effects also considered. The Semi analytic HAM is applied for said problems and obtained results of Momentum, energy and Concentration equations. velocity, temperature and concentration profiles. For better understanding of the problems, the velocity, temperature and concentration gradient is obtained and presented in tabular form.

Nomenclature:

B_0 Magnetic field	W_e local Weissenberg number.
u, v velocity component	p pressure
Nr Thermal Radiation	A ratio of velocities
θ Temperature profiles	c_1 rate of free stream velocity.
C Concentration profiles	φ Porosity of the porous medium
a stretching rate	Γ material time constant
D Mass diffusion coefficient	ν Kinematic viscosity coefficient
K_T thermal diffusion ratio	R_e local Reynolds number
Pr Prandtl number	Kr Chemical reaction parameter
M Magnetic parameter	H Heat generation Parameter
Sc Schmidt number	f dimensionless stream function
k_2 Chemical reaction	k_3 Thermal conductivity
k Permeability parameter	u_w stretching velocity
N buoyancy force parameter	η similarity variable
θ_w temperature ratio parameter	λ Mixed convection parameter
μ_0 viscosity at zero	Q_0 Heat absorption/generation coefficient
τ shear stress	I identity tensor
n power law exponent	

2. Formulation:

Here it is considered two-dimensional flow which is represented in Fig. 1 where, fluid temperature T_∞ and concentration C_∞. We assume that velocity $u_w(x) = ax$, temperature T_w and concentration C_w. The flow is considered in $y > 0$. The external magnetic field applied in y-direction.

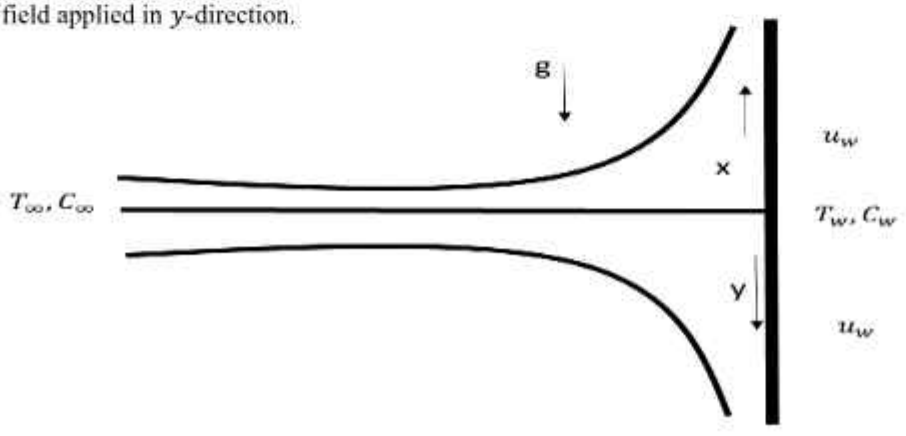

Figure 1: Physical Sketch

The Carreau fluid model is given by the following expression

$$\tau = -pI + \mu_0[(1 + (\Gamma\gamma)^2]^{\frac{n-1}{2}}.A_1 \tag{1}$$

When, $n = 1$ *or* $\Gamma = 0$ then it is considered as a Newtonian case.

Under all assumptions, the equations are as,

$$\frac{\partial u}{\partial x} + \frac{\partial v}{\partial y} = 0 \tag{2}$$

$$u\frac{\partial u}{\partial x} + v\frac{\partial u}{\partial y} = u_e\frac{du_e}{dx} + \nu\frac{\partial^2 u}{\partial y^2}\left[1 + {\lambda_1}^{*2}\left(\frac{\partial u}{\partial y}\right)^2\right]^{\left(\frac{n-1}{2}\right)} + \nu(n-1){\lambda_1}^{*2}\left[\frac{\partial^2 u}{\partial y^2}\left(\frac{\partial u}{\partial y}\right)^2\right]\left[1 + {\lambda_1}^{*2}\left(\frac{\partial u}{\partial y}\right)^2\right]^{\left(\frac{n-3}{2}\right)} - \sigma B_0^2(u_e - u) - \frac{\mu\varphi}{k_1}(u_e - u) + \rho g\beta_T(T - T_\infty) + \rho g\beta_C(C - C_\infty) \tag{3}$$

$$u\frac{\partial T}{\partial x} + v\frac{\partial T}{\partial y} = \frac{k_3}{\rho c_p}\frac{\partial^2 T}{\partial y^2} - \frac{1}{\rho c_p}\frac{\partial q_r}{\partial y} + \frac{Q_0}{\rho c_p}(T - T_\infty) \tag{4}$$

$$u\frac{\partial C}{\partial x} + v\frac{\partial C}{\partial y} = D\frac{\partial^2 C}{\partial y^2} - K_2(C - C_\infty) \tag{5}$$

$$u = u_w = ax,\ v = 0,\ T = T_w,\ C = C_w\ \ at\ y = 0. \tag{6}$$

$$u \to u_e = c_1 x, T \to T_\infty,\ \ C \to C_\infty;\ as\ \ y \to \infty \tag{7}$$

Using Rosseland approximation (1931), radiation heat flux $\mu_{nf} = \mu_{static} + \mu_{Brownian} = \frac{\mu_f}{(1-\phi)^{2.5}} + \frac{k_{Brownian}*\mu_f}{k_f*Pr_f}q_r$ can be written as

$$q_r = -\frac{16\sigma^*}{3k^*}T^3\frac{\partial T}{\partial y} \tag{8}$$

Differentiate (8) w.r.t y, we get

$$\frac{\partial q_r}{\partial y} = -\frac{16\sigma^*}{3k^*}\left[T^3\frac{\partial^2 T}{\partial y^2} + 3T^2\frac{\partial T}{\partial y}\right] \tag{9}$$

Input equation (9) in (5),

$$u\frac{\partial T}{\partial x} + v\frac{\partial T}{\partial y} = \frac{k_3}{\rho c_p}\frac{\partial^2 T}{\partial y^2} + \frac{1}{\rho c_p}\frac{16\sigma^*}{3k^*}\left[T^3\frac{\partial^2 T}{\partial y^2} + 3T^2\frac{\partial T}{\partial y}\right] + \frac{Q_0}{\rho c_p}(T - T_\infty) \tag{10}$$

The dimensionless variables are introduce,

$$\psi = \sqrt{\nu\, c_1}\, x f(\eta), T = T_\infty(1 + (\theta_w - 1)\theta),\ \ C(\eta) = \frac{C - C_\infty}{C_w - C_\infty},\ \eta = \sqrt{\frac{c_1}{\nu}}\, y,\ \ u = \frac{\partial\psi}{\partial y}, v = -\frac{\partial\psi}{\partial x}$$

Therefore, the governing equations dimensionless form are:

$$f'''\left[1 + n\,{W_e}^2 f''^2\right]\left[1 + {W_e}^2 f''^2\right]^{\left(\frac{n-3}{2}\right)} + f''f - f'^2 + \lambda(\theta + NC) + \left(M^2 + \frac{1}{k}\right)(1 - f') + A^2 = 0 \tag{11}$$

$$\theta'' + Nr\left[(1 + (\theta_w - 1)\theta)^3\theta'' + 3(\theta_w - 1)\theta'^2(1 + (\theta_w - 1)\theta)^2\right] + \frac{3Pr}{4}\theta' f + PrH\theta = 0 \tag{12}$$

$$C'' + Scf\ C' - Sc\ Kr\ C = 0 \tag{13}$$

subject to

$$f = 0, f' = 1, C = 1, \theta = 1\ at\ \eta = 0 \tag{14}$$

$$f' = A, C = 0, \theta = 0 \; at \; \eta \to \infty \tag{15}$$

where

$$W_e{}^2 = \frac{b^3 \lambda_1{}^{*2} x^2}{\nu}, \; A = \frac{c_1}{a}, \lambda = \frac{Gr_x}{{Re}^2}, N = \frac{Gr_x{}^*}{Gr_x}, Gr_x = \frac{g\beta_T (T_W - T_\infty)}{\nu^2} x^3, Gr_x{}^* = \frac{g\beta_C (C_W - C_\infty)}{\nu^2} x^3, R_e = \frac{x u_W}{\nu}, M^2 = \frac{\sigma {B_0}^2}{c_1 \rho}, Nr = \frac{16\sigma^* T^3_\infty}{3k^* k_3}, \frac{1}{Pr} = \frac{k_3}{\rho c_p}, Sc = \frac{\nu}{D}, \frac{1}{k} = \frac{\mu\varphi}{k_1}, \; Kr = \frac{K_2}{a}, \; H = \frac{Q_0 \nu^2}{\rho c_p}$$

3. HAM Solution:

To solve equations (11-13) simultaneously with conditions (14-15), the HAM suggested by Liao (2003) is employed.

Initial guess is given by:

$$f_0(\eta) = \eta A + (1 - A)(1 - e^{-\eta}); \theta_0(\eta) = e^{-\eta}; C_0(\eta) = e^{-\eta}; \tag{16}$$

with auxiliary linear operators:

$$L_f = \frac{\partial^3 f}{\partial \eta^3} - \frac{\partial f}{\partial \eta}, \; L_\theta = \frac{\partial^2 \theta}{\partial \eta^2} - \theta, L_C = \frac{\partial^2 C}{\partial \eta^2} - C \tag{17}$$

satisfying

$$L_f(C_1 + C_2 e^{\eta} + C_3 e^{-\eta}) = 0, \; L_\theta(C_4 e^{\eta} + C_5 e^{-\eta}) = 0, \quad L_C(C_6 e^{\eta} + C_7 e^{-\eta}) = 0. \tag{18}$$

where $c_1, \; c_2, \ldots, c_8$ are constants.

The zeroth order deformation problems are constructed as follows:

$$(1 - p) L_f[\hat{f}(\eta; p) - f_0(\eta)] = p\hbar_f N_f[\hat{f}(\eta; p), \hat{\theta}(\eta; p), \hat{C}(\eta; p)], \tag{19}$$

$$(1 - p) L_\theta[\hat{\theta}(\eta; p) - \theta_0(\eta)] = p\hbar_\theta N_\theta[\hat{f}(\eta; p), \hat{\theta}(\eta; p), \hat{C}(\eta; p)], \tag{20}$$

$$(1 - p) L_C[\hat{C}(\eta; p) - C_0(\eta)] = p\hbar_C N_C[\hat{f}(\eta; p), \hat{\theta}(\eta; p), \hat{C}(\eta; p)], \tag{21}$$

Subject to the boundary conditions:

$$\hat{f}(0; p) = 0, \quad \hat{f}'(0; p) = 1; \tag{22}$$

$$\hat{f}'(\infty; p) = A; \tag{23}$$

$$\hat{\theta}(0; p) = 1, \quad \hat{\theta}(\infty; p) = 0; \tag{24}$$

$$\hat{C}(0; p) = 1, \quad \hat{C}(\infty; p) = 0. \tag{25}$$

The nonlinear operator are defined as

$$N_f[\hat{f}(\eta; p), \hat{\theta}(\eta; p), \hat{C}(\eta; p)] = \frac{\partial^3 \hat{f}}{\partial \eta^3}\left[1 + nW_e{}^2 \left(\frac{\partial^2 \hat{f}}{\partial \eta^2}\right)^2\right]\left[1 + W_e{}^2 \left(\frac{\partial^2 \hat{f}}{\partial \eta^2}\right)^2\right]^{\left(\frac{n-3}{2}\right)} + \hat{f}\frac{\partial^2 \hat{f}}{\partial \eta^2}$$

$$- \left(\frac{\partial \hat{f}}{\partial \eta}\right)^2 + \lambda(\hat{\theta} + N\hat{C}) + \left(M^2 + \frac{1}{k}\right)\left(1 - \frac{\partial \hat{f}}{\partial \eta}\right) + A^2, \tag{26}$$

$$N_\theta[\hat{f}(\eta; p), \hat{\theta}(\eta; p), \hat{C}(\eta; p)] = \frac{\partial^2 \hat{\theta}}{\partial \eta^2} + \frac{3Pr}{4}\hat{f}\frac{\partial \hat{\theta}}{\partial \eta} + PrH\hat{\theta}$$

$$+Nr\left[\left(1 + (\theta_w - 1)\hat{\theta}\right)^3 \frac{\partial^2 \hat{\theta}}{\partial \eta^2} + 3(\theta_w - 1)\left(\frac{\partial \hat{\theta}}{\partial \eta}\right)^2 \left(1 + (\theta_w - 1)\hat{\theta}\right)^2\right], \tag{27}$$

$$N_C[\hat{f}(\eta; p), \hat{\theta}(\eta; p), \hat{C}(\eta; p)] = \frac{\partial^2 \hat{C}}{\partial \eta^2} + Sc\hat{f}\frac{\partial \hat{C}}{\partial \eta} - Sc \; Kr\hat{C} \tag{28}$$

Where $\hat{f}(\eta;\ p), \hat{\theta}(\eta;\ p)$ and $\hat{C}(\eta;\ p)$ are unknown functions with respect to η and p. $\hbar_f$, $\hbar_\theta$ and $\hbar_C$ are the non-zero auxiliary parameters and N_f, N_θ and N_C are the nonlinear operators.

Also $p \in (0,\ 1)$ is an embedding parameter. For $p = 0$ and $p = 1$ we have

$$\hat{f}(\eta; 0) = f_0(\eta), \hat{f}(\eta; 1) = f(\eta), \tag{29}$$

$$\hat{\theta}(\eta; 0) = \theta_0(\eta), \hat{\theta}(\eta; 1) = \theta(\eta), \tag{30}$$

$$\hat{C}(\eta; 0) = C_0(\eta), \hat{C}(\eta; 1) = C(\eta), \tag{31}$$

In other words, when variation of p is taken from 0 to 1 then $\hat{f}(\eta;\ p)$, $\hat{\theta}(\eta;\ p)$ and $\hat{C}(\eta;\ p)$ vary from $f_0(\eta), \theta_0(\eta)$, and $C_0(\eta)$ to $f(\eta), \theta(\eta)$, and $C(\eta)$. Taylor's series expansion of these functions yields the following:

$$\hat{f}(\eta;\ p) = f_0(\eta) + \sum_{m=1}^{\infty} f_m(\eta)p^m, \tag{32}$$

$$\hat{\theta}(\eta;\ p) = \theta_0(\eta) + \sum_{m=1}^{\infty} \theta_m(\eta)p^m, \tag{33}$$

$$\hat{C}(\eta;\ p) = C_0(\eta) + \sum_{m=1}^{\infty} C_m(\eta)p^m, \tag{34}$$

Where

$$f_m(\eta) = \frac{1}{m!}\left[\frac{\partial^m f(\eta; p)}{\partial p^m}\right]_{p=0}, \tag{35}$$

$$\theta_m(\eta) = \frac{1}{m!}\left[\frac{\partial^m \theta(\eta; p)}{\partial p^m}\right]_{p=0}, \tag{36}$$

$$C_m(\eta) = \frac{1}{m!}\left[\frac{\partial^m C(\eta; p)}{\partial p^m}\right]_{p=0}, \tag{37}$$

It should be noted that the convergence in the above series strongly depends upon $\hbar_f, \hbar_\theta$ and $\hbar_C$. Assuming that these nonzero auxiliary parameters are chosen so that Eqs.(32)-(34) converges at $p = 1$, Hence one can obtain the following:

$$f(\eta) = f_0(\eta) + \sum_{m=1}^{\infty} f_m(\eta), \tag{38}$$

$$\theta(\eta) = \theta_0(\eta) + \sum_{m=1}^{\infty} \theta_m(\eta), \tag{39}$$

$$C(\eta) = C_0(\eta) + \sum_{m=1}^{\infty} C_m(\eta), \tag{40}$$

Differentiating the zeroth order deformation (19) – (21) and (22) – (25) m times with respect to p and substituting $p = 0$, and finally dividing by !, we obtain the m^{th} order deformation $(m \geq 1)$.

$$L_f[f_m(\eta) - \chi_m f_{m-1}(\eta)] = \hbar_f R_{f,m}(\eta), \tag{41}$$

$$L_\theta[\theta_m(\eta) - \chi_m \theta_{m-1}(\eta)] = \hbar_\theta R_{\theta,m}(\eta), \tag{42}$$

$$L_C[C_m(\eta) - \chi_m C_{m-1}(\eta)] = \hbar_C R_{C,m}(\eta), \tag{43}$$

Subject to the boundary conditions

$$f_m(0) = 0, \tag{44}$$

$$f_m'(0) = f_m'(\infty) = 0, \tag{45}$$

$$\theta_m(0) = \theta_m(\infty) = 0, \tag{46}$$

$$C_m(0) = C_m(\infty) = 0, \tag{47}$$

with

$$R_{f,m}(\eta) = f'''_{m-1}\left[1 + n\,W_e{}^2 \sum_{j=0}^{m-1} f_j'^2\right]\left[1 + W_e{}^2 \sum_{j=0}^{m-1} f_j'^2\right]^{\left(\frac{n-3}{2}\right)} + \sum_{j=0}^{m-1} f_j f''_{m-1-j}$$

$$- \sum_{j=0}^{m-1} f_j'^2 + \lambda(\theta_{m-1} + NC_{m-1}) + \left(M^2 + \frac{1}{k}\right)(1 - f'_{m-1}) + A^2 \tag{48}$$

$$R_{\theta,m}(\eta) = \theta''_{m-1} + \frac{3Pr}{4} \sum_{j=0}^{m-1} f_j \theta'_{m-1-j} + PrH\theta_{m-1}$$

$$+Nr\left[(1 + (\theta_w - 1)\theta_{m-1})^3 \sum_{j=0}^{m-1} \theta_j'^2 + 3(\theta_w - 1) \sum_{j=0}^{m-1} \theta_j'^2 (1 + (\theta_w - 1)\theta_{m-1})^2\right] \tag{49}$$

$$R_{C,m}(\eta) = C''_{m-1} + Sc \sum_{j=0}^{m-1} f_j C'_{m-1-j} - Sc\,Kr\,C_{m-1} \tag{50}$$

$$\text{with } \chi_m = \{0, m \leq 1\ 1, m \geq 1\ , \tag{51}$$

Solving the corresponding m^{th}-order deformation equations,

$$f_m(\eta) = f_m^*(\eta) + C_1 + C_2 e^{\eta} + C_3 e^{-\eta} \tag{52}$$

$$\theta_m(\eta) = \theta_m^*(\eta) + C_4 e^{\eta} + C_5 e^{-\eta} \tag{53}$$

$$C_m(\eta) = C_m^*(\eta) + C_6 e^{\eta} + C_7 e^{-\eta} \tag{54}$$

Here $f_m^*, \theta_m^*\ and\ C_m^*$ are given by are particular solutions of the corresponding m^{th}-order equations and the constants $C_i(\ i = 1,2, \ldots,7)$ are to be determined by the boundary conditions.

4. Skin friction, Nusselt Number and Sherwood Number:

$$R_e{}^{\frac{1}{2}} C_{fx} = \left[1 + W_e{}^2 f''(0)^2\right]^{\left(\frac{n-1}{2}\right)} f''(0), \tag{55}$$

$$R_e{}^{-\frac{1}{2}} Nu = -\left(1 + R\theta_w{}^3\right)\theta'(0)\ \ and \tag{56}$$

$$R_e{}^{-1/2} Sh = -C'(0) \tag{57}$$

5. Convergence:

The HAM solutions depending the values of $\hbar_f, \hbar_\theta$ and $\hbar_C$. For this purpose, h-curves are plotted which is represented in Fig. 2- 4 respectively. These figures clearly advise suitable ranges for the auxiliary limits.

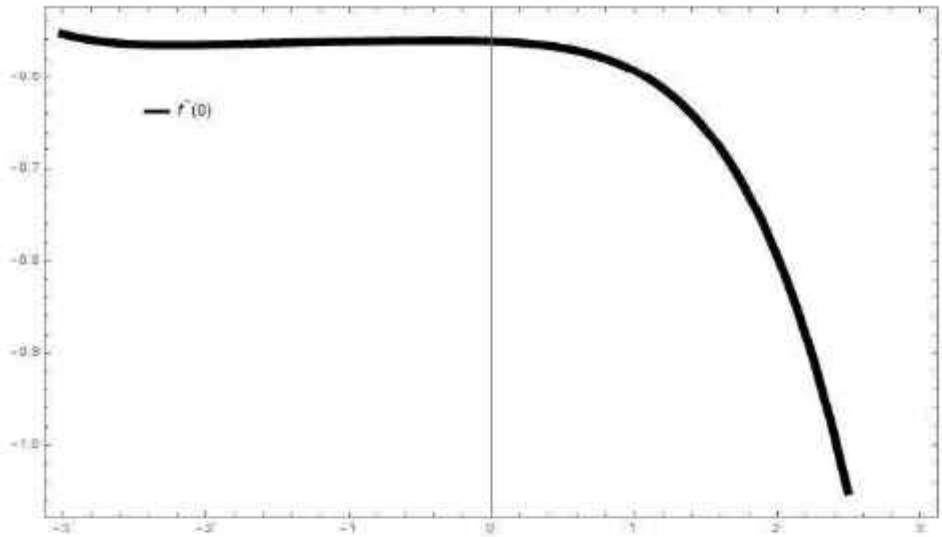

Figure 2: h-curve for $f''(0)$

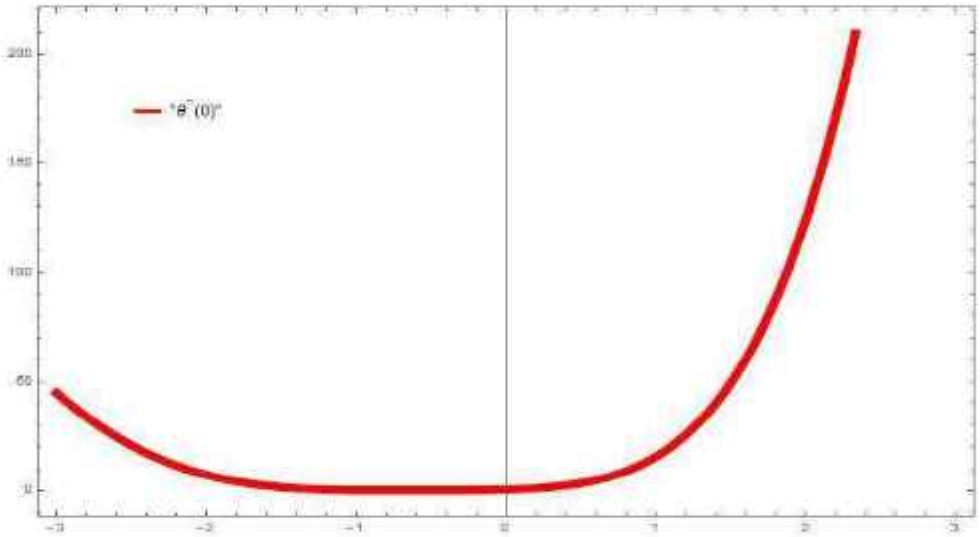

Figure 3: h-curve for $\theta'(0)$

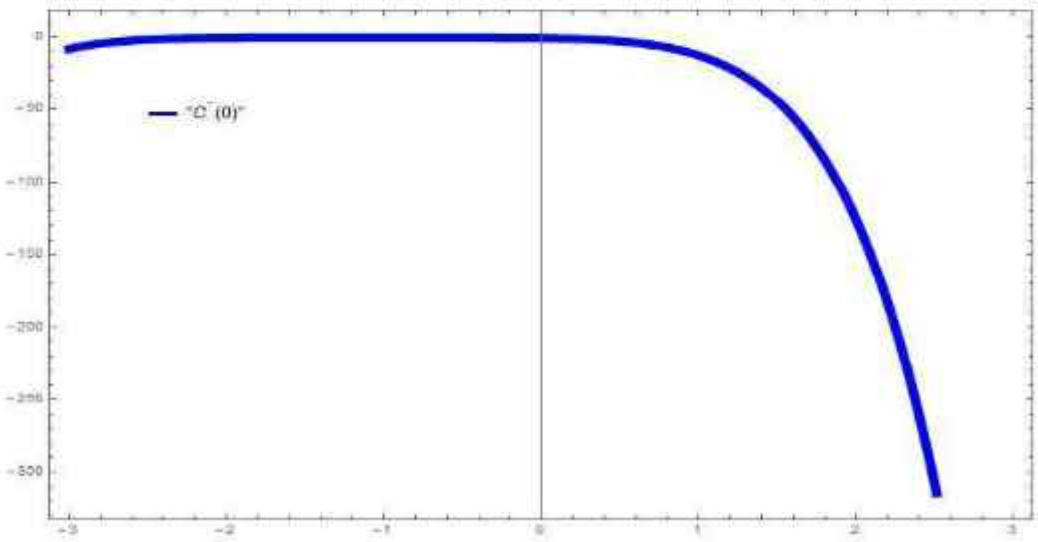

Figure 4: h-curve for $C'(0)$

6. Discussion of Results:

For this study, it is obtained velocity, temperature and concentration profiles for the case Non-Newtonian Carreau fluid ($n = 3$) which is represented in Fig. 5 to 14. Fig. 5 shows the effects of different values of A on velocity profiles. From the figures, it is seen that the velocity behaviour is different for $A > 1$ and $A < 1$ and there is no boundary layer for the values of $A = 1$. It is also concluded that the velocity profiles increases when ratio of velocity parameter is increase. Fig. 6 show the effect of M on velocity profiles. It is observed that the velocity improves with M. The physical reason behind this is because fluids with larger magnetic properties have stronger Lorentz forces, which make it harder for the fluid to move or, put another way, the flow slows down because the drag force is greater. The momentum and therma l layer thickness are also decreases for higher value of M. The effects of k on velocity profiles which is represented in Fig. 7. Physically, the fluid motion improves with increasing the values of k. So, this result is agreed with real situation. So, it is depicted that motion of the flow improve with k. Fig. 8 considered as the effects of We on velocity profiles. From the fig., it is seen that the motion of the fluid is slow down. Physically when increase the values of We, fluid become thick, due to this the flow motion delayed. Fig. 9 and Fig. 10 show the effects of λ and N on velocity profiles. Form both figures it is depicted that the motion of the fluid improves with both parameter values improve. Fig. 11 to 13 show the effects of Nr, θ_w and H on temperature profiles. Form all figures, it is concluded that the heat transfer process is increase with increases Nr, θ_w and H. Physically, when we raise the values of Nr or H, fluid become thin due to this reason the porosity will increase and hence heat transfer process improve. Fig. 14 show the effects of Kr on concentration parameter. From the figure it is concluded that the Kr tends reduced mass transfer process.

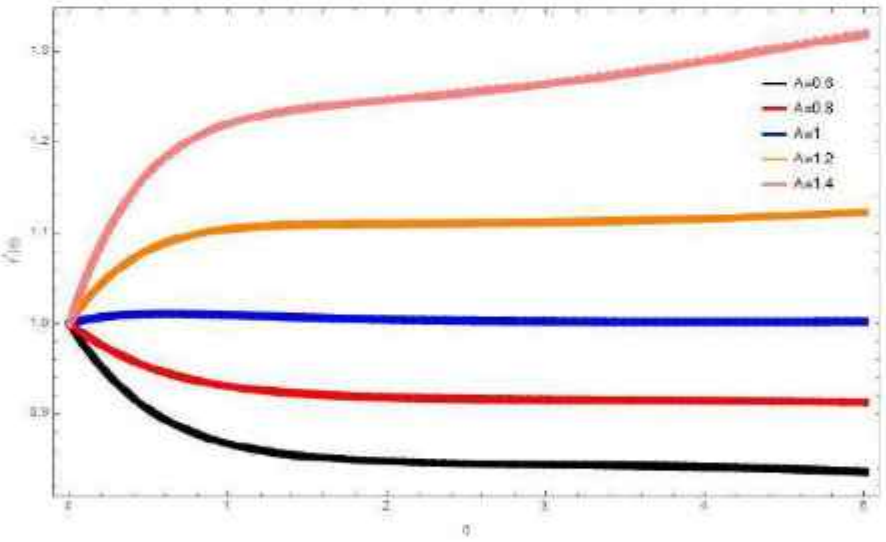

Figure 5: $f'(\eta)$ **for** A

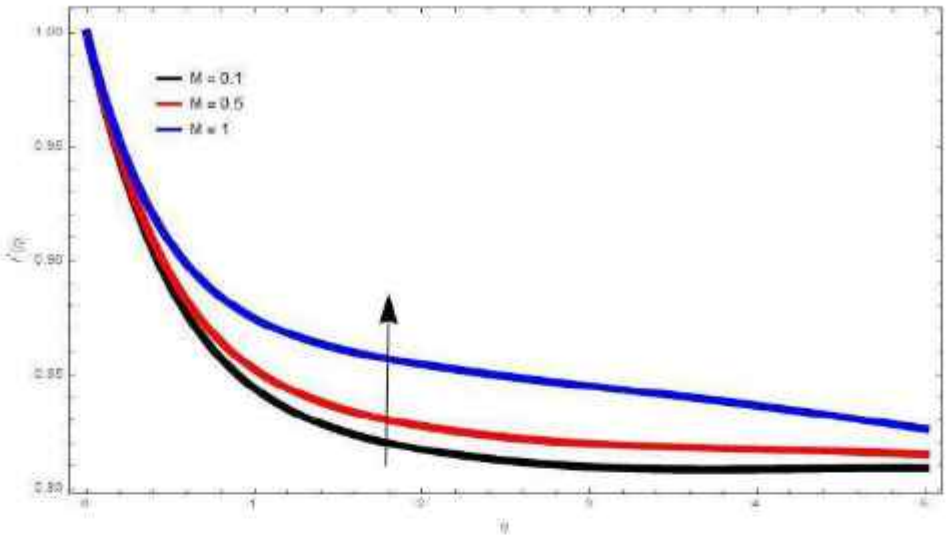

Figure 6: $f'(\eta)$ **for** M

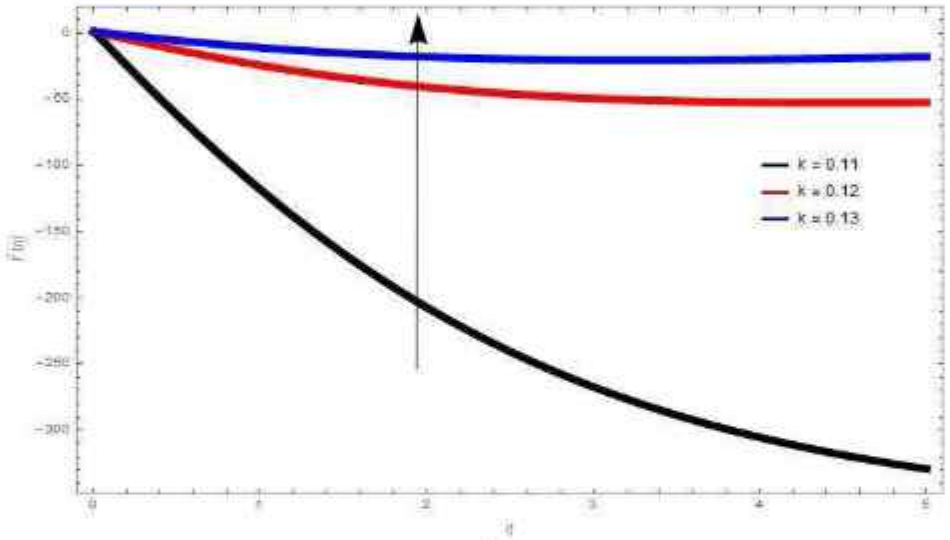

Figure 7: $f'(\eta)$ **for** k

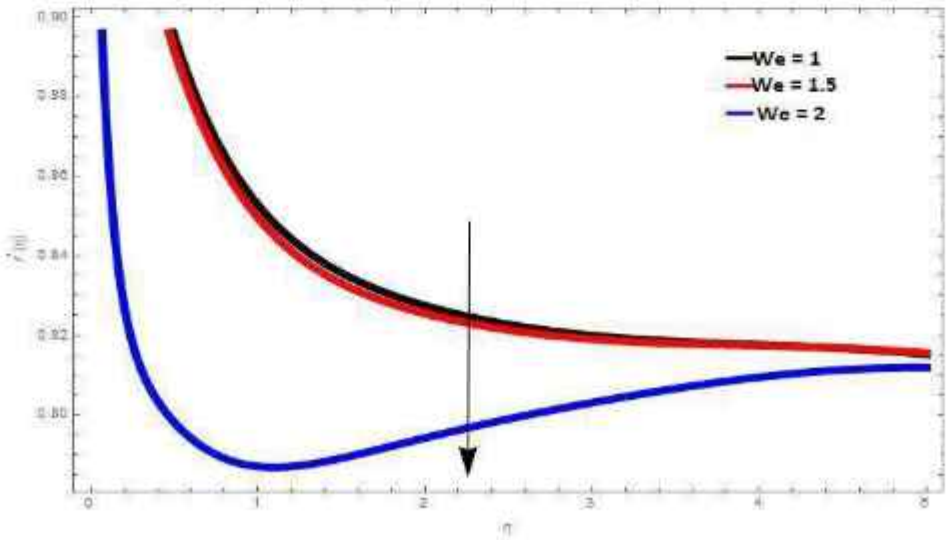

Figure 8: $f'(\eta)$ **for** W_e

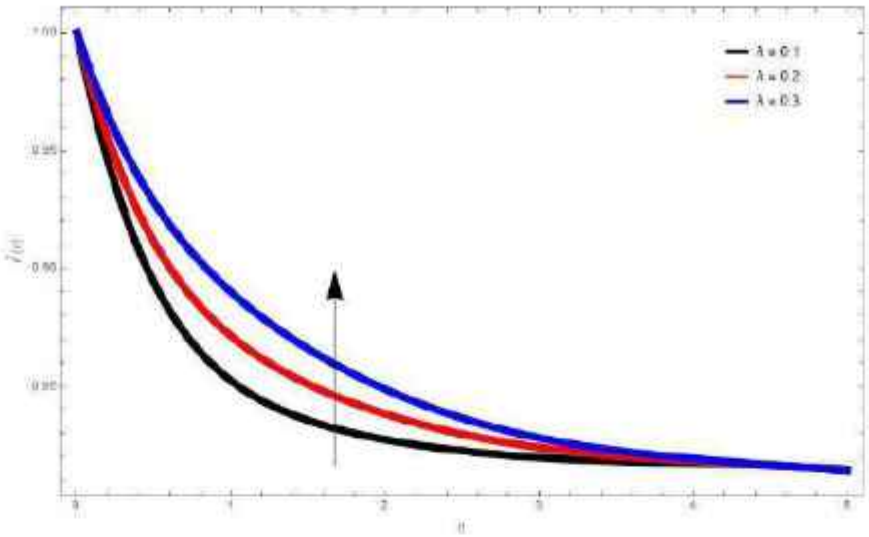

Figure 9: $f'(\eta)$ **for** λ

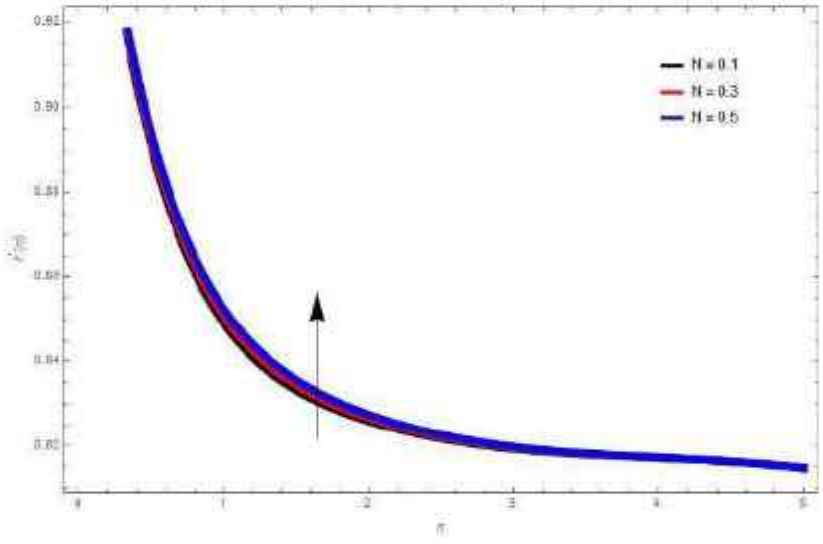

Figure 10: $f'(\eta)$ **for** N

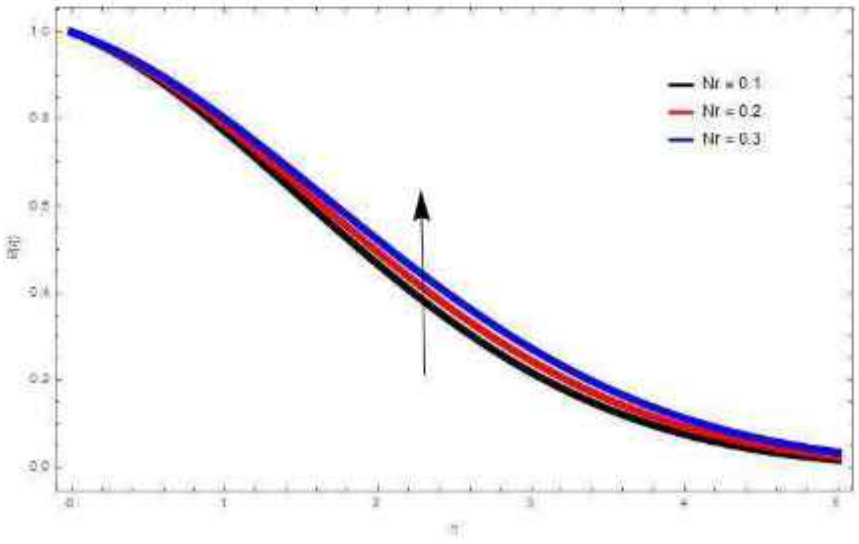

Figure 11: $\theta(\eta)$ **for** Nr

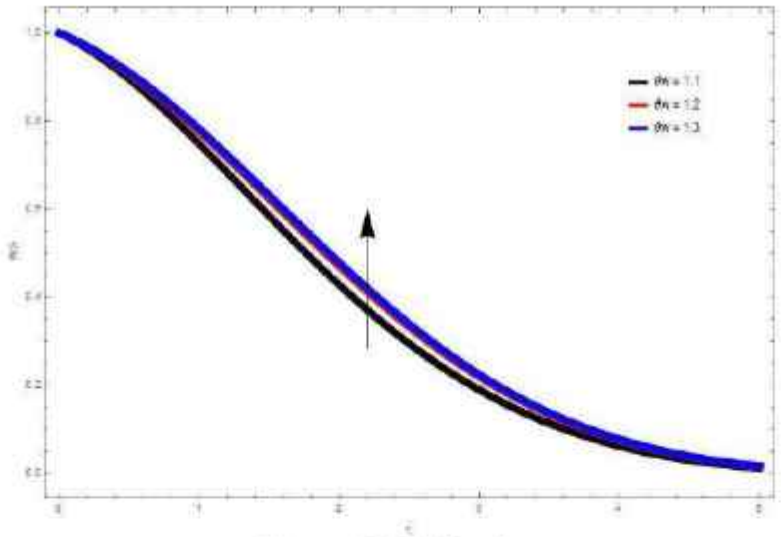

Figure 12: $\theta(\eta)$ **for** θ_w

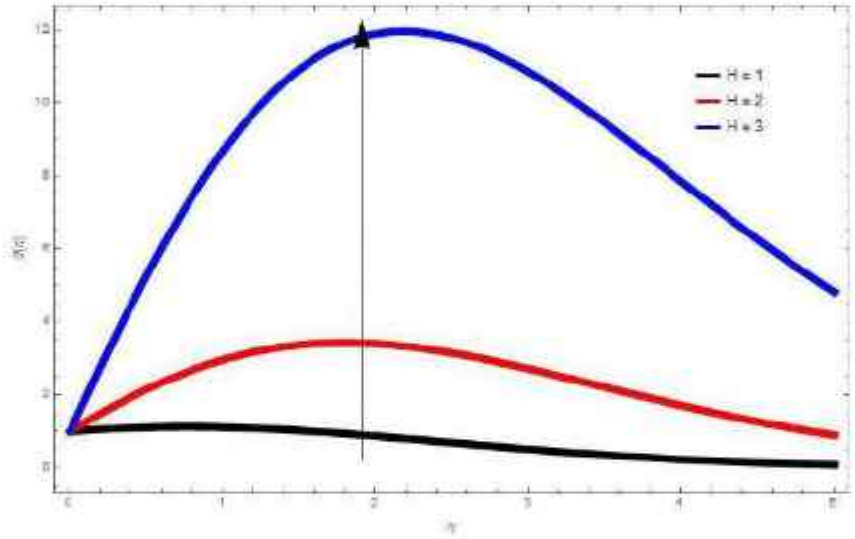

Figure 13: $\theta(\eta)$ **for** H

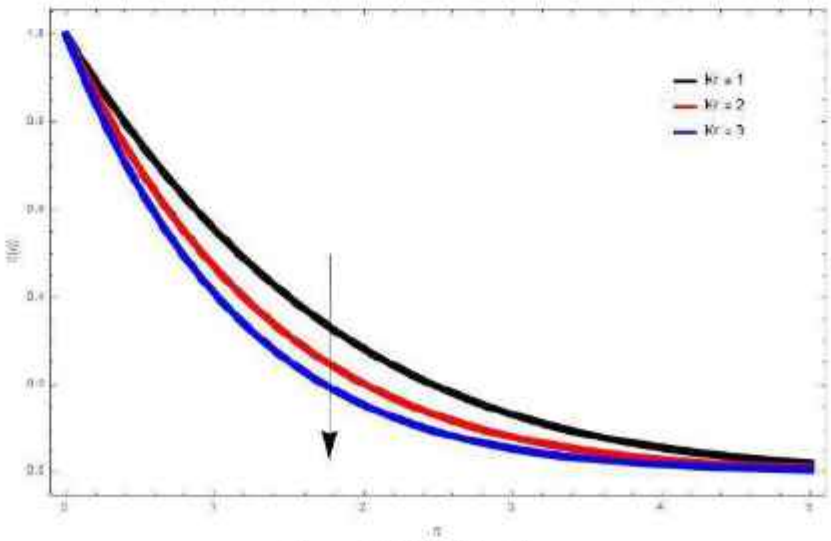

Figure 14: $C(\eta)$ **for** Kr

Table 1: Skin friction variation at $A = 0.5,\ n = 3, Sc = 0.22, Kr = 2, H = 1,$ $\theta_w = 1.2$ and $Pr = 0.5$.

M	k	N	λ	W_e	$R_e^{1/2} C_{fx} = \left[1 + W_e^2 f''(0)^2\right]^{\left(\frac{n-1}{2}\right)} f''(0)$
0.5	0.5	0.5	0.1	1.2	−0.3410154419552631
0.6					−0.3396249091928987
0.7					−0.339602089134368
	0.6				−0.3516693841805077
	0.7				−0.364257354004312
		0.6			−0.33733897337092467
		0.7			−0.33367304381176893
			0.2		−0.2682959929199615
			0.3		−0.19985309707142015
				1.3	−0.3583129522300399
				1.4	−0.39575808018451986

Table 2: Nusselt number at $A = 0.5,\ n = 3, Sc = 0.22, Kr = 2, M = 0.5, k = 0.5,$ $N = 0.5, \lambda = 0.1,$ and $W_e = 1.2$.

H	Nr	θ_w	Pr	$R_e^{-1/2} Nu = -\left(1 + R\theta_w^3\right)\theta'(0)$
1	0.1	1.2	0.5	−0.3822349948202121
1.1				−0.5313278140033504
1.2				−0.6982515781078514
	0.2			−0.34035128456534236
	0.3			−0.3397559491341102
		1.3		−0.38202051998804726
		1.4		−0.3817556335182837
			0.6	−0.5226596029294244
			0.7	−0.6655683887931871

Table 3: Sherwood number variation at $A = 0.5,\ n = 3, M = 0.5, k = 0.5, N = 0.5,$ $\lambda = 0.1, H = 1, Nr = 0.1, Pr = 0.5, \theta_w = 1.2$ and $W_e = 1.2$.

Sc	Kr	$R_e^{-1/2} Sh = -C'(0)$
0.2	2	0.72089585612932
0.3		0.84229051956253
0.4		0.97303001557467
	2.1	0.73592662849936
	2.2	0.75066331411672

Table 4: Comparison of the present results for Skin friction variation at

$$A = 0,\ n = 1, M = 0, Nr = 0, Pr = 0, \theta_w = 0 \text{ and } W_e = 0.$$

λ	Mahapatra & Nandy (2012)	Present Study
0.0	1.232588	1.232588
0.1	1.146560	1.146560
0.2	1.051131	1.051130
0.5	0.713296	0.713294

The deviation of the $R_e^{\frac{1}{2}}C_{fx}$, $R_e^{\frac{1}{2}}Nu$ and $R_e^{\frac{1}{2}}Sh$ is shown in Table 1 to 3. Table 1 show the effects of different values of M, k, λ, N and We on variation of $R_e^{\frac{1}{2}}C_{fx}$. From Table 1, it is depicted that the intensity of the velocity gradient improves with k and We whereas, reduced with M, λ *and* N. Table 2 indicate the values of temperature gradient for different values of Nr, H and θ_w. From this table, it is seen that H and Pr tends to improve the magnitude of temperature gradient whereas, Nr and θ_w have opposite effect on it. Table 3 shows Kr and Sc effects on concentration gradient. From this table, it is concluded that the rate of mass transfer increase with Kr and Sc. To check the validation of present studies, Numerical values of local skin friction is compared with previous published works in a special case which is presented in Table 4. Form this table, it is concluded that the present results are strongly agree with published works Mahapatra & Nandy (2012)

7. Conclusion:

The main conclusion points are as follows

- The various values of velocity ratio parameter effects on velocity profiles have different behaviour.
- Magnetic field and permeability of porous medium parameter tends to improve the fluid motion whereas, local Weissenberg number have reverse effect on it.
- The motion of fluid has increase when the values of mixed convection parameter as well as buoyancy force parameter increased.
- Heat transfer process increase with thermal radiation, thermal ratio parameter and heat generation parameter.
- The growing values of chemical reaction parameter tends to restrict the mass transfer process.
- The magnitude of the skin friction improves with porosity and local Weissenberg number whereas, reduced with magnetic field, buoyancy force and mixed convection parameter.
- Heat generation parameter tends to improve the magnitude of Nusselt Number whereas, thermal radiation parameter and temperature ratio parameter have reverse effect on it
- The rate of mass transfer increase with chemical reaction parameter.

REFERENCES:

- Jiann, L.Y., Mohamad, A. Q., Rawi, N. A., Ching, D. L. C., Zin, N. A. M., & Shafie, S. (2024): Thermal analysis of melting effect on Carreau fluid flow around a stretchable cylinder with quadratic radiation, Propulsion and Power Research, 13(1), 132-143.
- Vaidya, H., Tripathi, D., Mebarek-Oudina, F., Rajashekhar, C., Baskonus, H. M., Prasad, K. V., & Shivaleela, (2024): Scrutiny of MHD impact on Carreau Yasuda (CY) fluid flow over a heated wall of the uniform micro-channel, Chinese Journal of Physics, 87, 766-781.
- Rehman, K. U., Shatanawi, W., & Colak, A. B. (2024): Neural networking-based analysis of heat transfer in MHD thermally slip Carreau fluid flow with heat generation, Case Studies in Thermal Engineering, 54, 103995.
- Salahuddin, T., Awais, M., & Raza, M. I. (2024): Thermophysical characteristics with natural convective flow of Carreau fluid influencing by Soret and Dufour effects: By using numerical technique, International Journal of Thermofluids, 21, 100589.
- Ming, C., Liu, K., Han, K., & Xinhui Si, (2023): Heat transfer analysis of Carreau fluid over a rotating disk with generalized thermal conductivity, Computers & Mathematics with Applications, 144, 141-149.
- Kudenatti, R. B., Misbah, N. E., & Bharathi, M. C. (2023): A numerical study on boundary layer flow of Carreau fluid and forced convection heat transfer with viscous dissipation and generalized thermal conductivity, Mathematics and Computers in Simulation, 208, 619-636.
- Almaneea, A. (2024): Computational investigation on transport of heat energy by flow of dusty Carreau fluid with nanoparticles using finite element method, Ain Shams Engineering Journal, 15, 102377.
- Salahuddin, T., & Awais, M. (2022): A comparative study of Cross and Carreau fluid models having variable fluid characteristics, International Communication in Heat and Mass Transfer, 139, 106431.
- Khan, M., Salahuddin, T., & Chu, Y. M. (2021): Analysis of the Carreau fluid model presenting physical properties along different molecular axes near an anisotropic rough surface, International Communication in Heat and Mass Transfer, 123, 105233.
- Salahuddin, T., Javed, A., Khan, M., Awais, M., & Bangali, H. (2022): The impact of Soret and Dufour on permeable flow analysis of Carreau fluid near thermally radiated cylinder, International Communication in Heat and Mass Transfer, 138, 106378.
- Li, S., Faizan, M., Ali, F., Ramasekhar, G., Muhammad, T., Khalifa, H. A. E., & Ahmad, Z. (2024): Modelling and analysis of heat transfer in MHD stagnation point flow of Maxwell nanofluid over a porous rotating disk, Alexandria Engineering Journal, 91, 237-248.
- Alqahtani, S., Hashim, Rehman, S., Kainat, & Alshehery, S. (2023): Computational method for energy transport of MHD nanofluids flow near non-aligned stagnation point with non-linear thermal radiation and interface slip, Results in Engineering, 19, 101383.
- Mittal, A., Patel, H., Patoliya, R. & Gohil, V. (2024): Effects of magnetic field and chemical reaction on a time dependent Casson fluid flow, Applications and Applied Mathematics: An International Journal (AAM) 19 (3), 8
- Mittal, A. & Kori, V. (2024): Impact of Dufour-Soret Diffusion and Chemical Reactivity on Darcy-Forchheimer MHD Nanofluid Flow Over a Variable-Thickness Elastico-Viscous Sheet, International Journal of Applied and Computational Mathematics 11, 28
- Patel, H., Mittal, A. & Nagar, T. (2024): Thermo-Diffusion and Heat Generation Effects on Unsteady MHD Flow of Nanofluid in a Perforated Vertical Medium, Fluid Mechanics and Fluid Power, 303-319
- Patel, H., Mittal, A. & Nagar, T. (2024): Effect of magnetic field on unsteady mixed convection micropolar nanofluid flow in the presence of nonuniform heat source/sink, International Journal of Ambient Energy 45 (1), 2266748
- Patel, H., Mittal, A. & Nagar, T. (2022): Fractional order simulation for unsteady MHD nanofluid flow in porous medium with Soret and heat generation effects, Heat Transfer 52 (1), 563-584
- Alrehili, M. (2024): Nanofluid dissipative stagnation point flow of Casson type over a stretched sheet influenced by a variable surface heat flux and magnetic field, Results in Physics, 58, 107535.
- Swain, S., Sarkar, G. M., & Sahoo, B. (2024): Stability analysis of MHD stagnation point flow of Casson fluid past a shrinking sheet in porous medium considering heat sink or source, thermal radiation and suction effects, Journal of Computational Science, 75, 102207.
- Rafique, K., Mahmood, Z., Alqahtani, A. M., Elsiddieg, A. M. A., Khan, U., Deebani, W., & Shutaywi, M. (2023): Impacts of thermal radiation with nanoparticle aggregation and variable viscosity on unsteady bidirectional rotating stagnation point flow of nanofluid, Materials Today Communications, 36, 106735.

- Zaheer, M., Abbas,S. Z., Huang, N., & Elmasry, Y. (2024): Analysis of buoyancy features on magneto hydrodynamic stagnation point flow of nanofluid using homotopy analysis method, International Communication in Heat and Mass Transfer, 221, 125045.
- Baig, M. N. J., Salamat, N., Duraihem, F. Z., Akhtar, S., Nadeem, S., Alzabut, J., & Saleem, S. (2023): Exact analytical solutions of stagnation point flow over a heated stretching cylinder: A phase flow nanofluid model, Chinese Journal of Physics, 86, 1-11.
- Siddiqi, M. T., Safdar, Dutt, H. M., Taj, S., Khan, M. I., Abdullaeva, B. S., Altuijri, R., & Hassan, A. M. (2023): Comparative analysis of analytical and numerical approximations for the flow and heat transfer in mixed convection stagnation point flow of Casson fluid, Results in Physics, 52, 106819.
- Waqas, H., Alqarni, M. S., Muhammad, T., & Khan, M. A.(2021): Numerical study for bioconvection transport of micropolar nanofluid over a thin needle with thermal and exponential space-based heat source, Case Studies in Thermal Engineering, 26, 1-12.
- Mittal, A. S., Patel, H. R., & Darji, R. R. (2019): Mixed convection micropolar ferrofluid flow with viscous dissipation, joule heating and convective boundary conditions, International Communications in Heat and Mass Transfer, 108, 104320.
- Jalili, B., Jalili, P., Sadighi, S., & Ganji, D. D. (2021): Effect of magnetic and boundary parameters on flow characteristics analysis of micropolar ferrofluid through the shrinking sheet with effective thermal conductivity, Chinese Journal of Physics, 71, 136-150.
- Patel, H. R., Mittal, A. S., & Darji R. R. (2019): MHD flow of micropolar nanofluid over a stretching/shrinking sheet considering radiation, International Communications in Heat and Mass Transfer, 108, 104322.
- Gumber, P., Yaseen, M., Rawat, S. K., & Kumar, M. (2022): Heat transfer in micropolar hybrid nanofluid flow past a vertical plate in the presence of thermal radiation and suction/injection effects, Partial Differential Equations in Applied Mathematics, 5, 100240.
- Kausar, M. S., Hussanan, A., Waqar, M., & Mamat, M. (2022): Boundary layer flow of micropolar nanofluid towards a permeable stretching sheet in the presence of porous medium with thermal radiation and viscous dissipation, Chinese Journal of Physics, 78, 435-452.
- Khader, M. M. (2019): Fourth-order predictor-corrector FDM for the effect of viscous dissipation and Joule heating on the Newtonian fluid flow, Computers & Fluids, 182, 9-14.
- Patel, H. R., & Singh, R. (2019): Thermophoresis, Brownian motion and non-linear thermal radiation effects on mixed convection MHD micropolar fluid flow due to nonlinear stretched sheet in porous medium with viscous dissipation, joule heating and convective boundary condition, International Communications in Heat and Mass Transfer, 107, 68-92.
- Patel, H. R., Patel, S. D., & Darji, R. R. (2022): Mathematical Study of unsteady micropolar fluid flow due to non-linear stretched sheet in the presence of magnetic field, International Journal of Thermofluids, 16, 100232.
- Simon, J. S. H., & Notsu, H. (2022): A convective boundary condition for the Navier–Stokes equations, Applied Mathematics Letters, 128, 107876.
- Wahid, N. S., Arifin, N. M., N. S. Khashie, N. S., Pop, L., Bachok, N., & Hafidzuddin, M. E. H. (2022): Unsteady MHD mixed convection flow of a hybrid nanofluid with thermal radiation and convective boundary condition, Chinese Journal of Physics, 77, 378-392.
- Han, W. W., Chen, H. B., & Lu, T. (2019): Estimation of the time-dependent convective boundary condition in a horizontal pipe with thermal stratification based on inverse heat conduction problem, International Journal of Heat and Mass Transfer, 132, 723-730.
- Rosseland, S. (1931): Astrophysik und atom-theoretischeGrundlagen, Springer-Verlag, Berlin.
- Liao, S. J. (2003): Beyond perturbation: Introduction to homotopy Analysis Method, Chapman and Hall/CRC Press, Boca Raton.
- Mahapatra, T. R., & Nandy, S. K. (2012). Stability of dual solutions in stagnation-point flow and heat transfer over a porous shrinking sheet with thermal radiation. Meccanica, 48(1), 23–32.